RSC Advances

ROYAL SOCIETY OF CHEMISTRY

www.rsc.org/advances

Novel solid-solid phase change materials with biodegradable trihydroxy surfactant for thermal energy storage

Xiaowei Fu[a], Weibo Kong[a], Yanyan Zhang[a], Liang Jiang[a], Jiliang Wang[b], Jingxin Lei[a,*]

[a] *State Key Laboratory of Polymer Materials Engineering, Polymer Research Institute of Sichuan University, Chengdu 610065, China*

[b]*School of Chemistry Science and Engineering, Yunnan University, Kunming 650091, China*

**Corresponding author: Jingxin Lei; Email: jxlei@scu.edu.cn; Tel: +86-28-85401152; Fax: +86-28-85404920*

Abstract

Polyurethane polymers were synthesized as novel solid-solid phase change materials (SSPCMs) by bulk polycondensation in the absence of organic solvents, in which the polyethylene glycol (PEG) was selected as phase change working substance and the Span 80 and Tween 80 was used as crosslinking agents for the first time. The chemical structures, crystalline properties, phase change properties and thermal stability of the synthesized SSPCMs were characterized by Fourier transform infrared spectroscopy (FTIR), X-ray diffraction (XRD), differential scanning calorimetry (DSC) and thermogravimetric analysis (TG). An accelerated thermal cycling testing was carried out to reveal the thermal reliability of the synthesized SSPCMs. The XRD patterns showed the synthesized SSPCMs have a completely crystalline structure and

the defective crystallization compared with the pristine PEG. The DSC results denoted the synthesized SSPCMs have the proper phase change temperatures of 37-48 ℃ and high latent heats in the range of 120 -130 J/g. TG results shows the synthesized SSPCMs possess good thermal stability.

1. Introduction

In recent years, energy crisis derived from the shortage of mineral resources and continuous deterioration of environment becomes a global issue.[1,2] For that, the phase change materials (PCMs) for thermal energy storage (TES) have drawn the increasing attention from both academia and industry.[3-5] PCMs can absorb and release a large amount of heat during the phase change process with small temperature fluctuation and high energy storage density.[6-8] Therefore, PCMs for TES can be widely applied in such fields as heat transfer fluid[9], thermal regulation[10], building materials[11], waste heat recovery[12] and solar energy storage[13]. Compared with the solid-liquid PCMs such as paraffin[14,15] and fatty acid[16,17], the polymeric solid-solid PCMs have very big advantages of no leakage when used, easiness to use and needless encapsulation.[18-20] Thus, the polymeric solid-solid PCMs have been developed and studied by polymer encapsulation (i.e. form-stable PCMs),[21-23] graft polymerization[24] and block polymerization[19].

Based on the advantages of solid-solid PCMs, some attempts have been made to synthesize the outstanding polymer-based PCMs. Su et al.[25] prepared polyurethane block copolymer as solid-solid PCMs by solution polycondensation, which was

composed of high molecule weight polyethylene glycol (PEG) as soft segment, 4,4'-diphenylmethane diisocyanate (MDI) and 1,4-butanediol (BDO) as a chain extender. Sari et al.[24,26] synthesized polystyrene-graft-palmitic acid and polystyrene-graft-PEG copolymers as solid-solid PCMs by solution graft polymerization, where a large amount of dimethylformamide (DMF) were used to reduce the viscosity of the reaction system. Chen et al.[27] prepared novel polyurethane-based solid-solid PCMs with different hexahydroxy compounds using sorbitol, dipentaerythritol and inositol as crosslinking agents. For the solution polycondensation method, the preparation process involved a large number of DMF organic solvent. Xi et al.[28] reported the synthesis of thermoplastics polyurethane solid-solid PCMs by a newly synthesized tetrahydroxy compound, bis(1,3-dihydrox-ypropan-2-yl) 4,4'-methylenebis (4,1-phenylene)dicarbamate. In its molecular structure, the polyethylene glycol was employed as the soft segments, and the hard segments were made up of 4,4'-diphenylmethane diisocyanate and tetrahydroxy compound made up of multi-benzene ring structure. All of the above, high latent heats and proper phase change temperatures are of prime importance. However, a large number of organic solvents such as DMF were involved in the preparation process. Therefore, the synthesis of polymeric solid-solid PCMs in the absence of organic solvent will be a potential subject.

In this work, a novel solvent-free synthesis of solid-solid PCMs was developed with high phase change enthalpy and the phase change temperature less than 100 ℃. Meanwhile, the biodegradable trihydroxy surfactants, Span 80 and Tween 80, were

selected as the crosslinking agents, diphenylmethane diisocyanate (MDI) was used as the skeleton, and the high molecular weight PEG was served as the phase change functional chains in the solid-solid PCMs. In addition, the Span 80 and Tween 80 were used as reactants in polyurethane synthesis for the first time. It is believed that the biodegradable Span 80 and Tween 80 can potentially make good the biodegradability of synthesized solid-solid PCMs. The chemical composition, crystalline properties, phase change properties and thermal stability of synthesized solid-solid PCMs were studied by Fourier transform infrared spectroscopy (FTIR), X-ray diffraction (XRD), differential scanning calorimetry (DSC) and thermogravimetric analysis (TG). An accelerated thermal cycling testing to confirm the thermal reliability of solid-solid PCMs was conducted.

2. Experimental

2.1. Materials

Polyethylene glycol (PEG, analytical grade, M_n=6,000 g/mol, from Chengdu Kelong Chemical Reagent Company, China), Span 80 (from Tianjin Bodi Chemical Co., Ltd, China) and Tween 80 (from Tianjin Kemiou Chemical reagent Co., Ltd, China) were dried under vacuum at 110 ℃ for 3 h prior to use. Diphenylmethane diisocyanate (MDI-50, from Wanhua Chemical Group Co. Ltd., China) containing 50 wt% 4,4'-diphenylmethane diisocyanate and 50 wt% 2, 4'- diphenylmethane diisocyanate was used as received.

2.2. Synthesis of solid-solid PCMs

The solid-solid PCMs were synthesized under an inert atmosphere of nitrogen in the absence of organic solvents by a consecutive bulk polycondensation and the corresponding synthetic route is shown in Fig. 1. Firstly, a predetermined amount of PEG and MDI-50 (molar ratio of PEG and MDI-50 = 1:2) after homogenization was reacted with stirring at 80 ℃ for 3 h. Secondly, After cooled down to 70 ℃ the trihydroxy surfactant such as Span 80 and Tween 80 (molar ratio of ternary alcohol and MDI-50 = 1:3) was added into the above mixture, and then fully mixing was performed for 30 min. Thirdly, thermal curing was conducted at 90 ℃ for 6 h in a drying oven. Afterwards, the solid-solid PCMs via crosslinking reaction of trihydroxy surfactant were obtained.

The prepared solid-solid PCMs by Span 80 and Tween 80 crosslinking were labeled as SPCM and TPCM, respectively.

2.3. Characterization

2.3.1. Fourier transform infrared spectroscopy (FTIR). FTIR of PEG, Span 80, Tween 80, SPCM and TPCM was conducted to measure the chemical structures using infrared spectrometer (Nicolet 560, Nicolette Co., USA) with a resolution setting of 4 cm^{-1} and the scanning range from 4000 to 400 cm^{-1}. The KBr pressed disc technique (about 1mg KBr of sample and 100 mg of KBr) was used for sample preparation of PEG, Span 80 and Tween 80. SPCM and TPCM were measured by ATR (attenuated total reflection).

2.3.2. X-ray diffraction (XRD). The crystalline structures of PEG, SPCM and TPCM were investigated using automatic powder diffractometer (X'Pert pro MPD, Netherlands) with Cu Kα at 35 kV and 30 mA. The 2θ range was changed from 5 to 50° by a 0.04° step programmed with a collection time of 0.2 s per step.

2.3.3. Differential scanning calorimetry (DSC). The phase change temperatures and latent heats of PEG, SPCM and TPCM were investigated via a differential scanning calorimeter (DSC 204 F1, German) at 10 ℃/min under nitrogen atmosphere and around 10 mg of sample for each testing. To eliminate the heat history of materials before testing, each sample was suffered from a thermal cycle with a heating/cooling rate of 10 ℃/min (containing a heating process from 25 ℃ to 100 ℃ and then a cooling process from 100 ℃ to 25 ℃).

2.3.4. Thermogravimetric analysis (TG). The thermal stability of PEG, SPCM and TPCM was studied by a TA Instrument SDT-Q600 thermal analyzer (USA) from 25 to 600 ℃ under a nitrogen atmosphere. The heating rate was 10 ℃/min and about 10 mg of sample were needed for each testing. The obtained TGA results were analyzed by a TA universal analysis program.

2.3.5. Accelerated thermal cycling testing. To confirm the thermal reliability of the prepared SPCM and TPCM, the accelerated thermal cycling testing was performed in high-low temperature chamber.[20] The typical thermal cycling program was set with 100 consecutive heating and cooling process. The temperature was altered between 20 and 90 ℃ and each heating-cooling process was completed by 20 min with a respective 5 min isothermal at 20 ℃ and 90 ℃. After that, the phase

transition properties and chemical stability of SPCM and TPCM after thermal cycling were studied by DSC and FTIR analysis.

3. Results and discussion

3.1. FTIR results

To denote the chemical structures of the synthesized solid-solid PCMs, FTIR spectra of PEG, Span 80, Tween 80, SPCM and TPCM are shown in Fig. 2 and Table 1 summarizes the characteristic peaks and the corresponding characteristic vibration of PEG, Span 80 and Tween 80. In Fig. 2(a) and Table 1, the characteristic absorption band at 3481 cm^{-1} is ascribed to the stretching vibration of the O-H group and the C-O-C symmetric stretching vibration appear at 1101 cm^{-1}. The strong peaks at 2888 cm^{-1}, 1467 cm^{-1}, 1342 cm^{-1}, 1280 cm^{-1}, 1242 cm^{-1}, 962 cm^{-1} and 842 cm^{-1} are attributed to the C-H vibration. As seen from Fig. 2(b) and Table 1, the broad absorption band at 3399 cm^{-1} is resulted from the O-H stretching vibration. The C=O and C-O stretching vibration in ester group appear at 1739 cm^{-1} and 1173 cm^{-1}. The absorption peaks at 2925 cm^{-1} and 2855 cm^{-1} are ascribed to the stretching vibration of $–CH_2-$ and $–CH_3$. The bending vibration of $–CH_3$ occurs at 1459 cm^{-1} and 1374 cm^{-1}. The characteristic absorption peak at 1173 cm^{-1} is derived from the C-O-C stretching vibration. As shown in Fig. 2(c) and Table 1, the absorption band of –OH group appears at 3428 cm^{-1}. The sharp absorption peaks at 1735 cm^{-1} and 1107 cm^{-1} are attributed to the C=O and C-O stretching vibration of ester group, respectively. The absorption peaks of $–CH_2-$ group occur at 2923 cm^{-1}, 2864 cm^{-1}, 948 cm^{-1} and 842

cm^{-1}. It can be seen from Fig. 2(d) that the absorption peaks at 1739 cm^{-1} and 1085 cm^{-1} are respectively ascribed to the C=O and C-O stretching vibration in ester or urethane group. The absorption peaks of $–CH_2-$ group appear at 2879 cm^{-1}, 961 cm^{-1} and 842 cm^{-1}. The characteristic absorption peak at 1539 cm^{-1} is derived from the amide vibration of –NHCOO- groups. The characteristic absorption peaks from Fig. 2(e) are similar to what can be seen in Fig. 2(d). Together with the fact that the strong hydroxyl absorption peaks above 3000 cm^{-1} and characteristic absorption peak of isocyanate from MDI at 2265 cm^{-1} disappear[27,29], it can be concluded from the above discussion that solid-solid SPCM and TPCM have been successfully synthesized.

3.2. Crystalline properties of solid-solid PCMs

The XRD technique was employed to investigate the crystalline properties affecting the enthalpy of solid-solid PCM and Fig. 3 shows the XRD curves of PEG, SPCM and TPCM. In Fig. 3, each curve has strong diffraction peaks observed, indicating that each sample exhibits a completely crystalline structure. As shown in Fig. 3, PEG has two sharp diffraction peaks at 19.0° and 23.2° according with the interplanar spacing of 4.65 Å and 3.82 Å respectively, denoting that PEG has good crystalline properties. It can be seen from Fig. 3 that SPCM and TPCM have the same diffraction peaks at 19.0° and 23.2° as pristine PEG, testifying that there is uniform crystalline structure existing in PEG, SPCM and TPCM. Compared with pristine PEG, the blunt peaks and wide half width of diffraction peaks confirm the defective crystallization and the small grain of poly(ethylene oxide) soft segments in SPCM and TPCM due to

the crosslinking structure and the hard rigid benzene ring groups existing in SPCM and TPCM. It can be found that the intensity of diffraction peaks in SPCM and TPCM is lower than that in PEG because of the imperfect crystallizing. Depending on crystalline properties, the enthalpy of PEG, SPCM and TPCM can reflect the crystallinity, which will be discussed latter in DSC analysis.

3.3 Phase change properties of solid-solid PCMs

To study the phase change properties of solid-solid PCMs, the DSC analysis was conducted with the heating/cooling rate of 10 ℃/min according with most previous literatures[1,3,4,15,25,30-35]. Fig. 4 shows the DSC curves of PEG, SPCM and TPCM and the detailed melting and freezing temperatures and latent heats are presented in Table 2. In consideration of the liquid state at room temperature, Span 80 and Tween 80 were not characterized by DSC analysis. As shown in Fig. 4, PEG has sharp melting and freezing peaks, confirming the existence of good crystalline structure consistent of the XRD results in Fig. 3. The melting and freezing temperatures respectively appear at 59.7 ℃ and 39.6 ℃ and the melting and freezing latent heats reach up to 234.4 J/g and 248.1 J/g respectively in Table 2. Similar to previous reports of pristine PEG[19,25], the undercooling of 20 ℃ occurs, possibly due to the slow homogeneous nucleation. As a typical solid-liquid PCMs, the PEG changes from a white crystal solid to a transparent liquid once the temperature reaches 60 ℃. Compared with pristine PEG, SPCM and TPCM have blunt and broad DSC peaks in melting and freezing curves of Fig. 4, further testifying the defective crystal and small grain in

accordance with XRD results of SPCM and TPCM in Fig. 3. For SPCM shown in Table 2, the melting and freezing temperatures and latent heats are measured as 44.3 ℃ and 37.2 ℃ as well as 122.4 J/g and 120.3 J/g respectively, meaning that the solid-solid PCMs will absorb thermal energy when the temperature is higher than 44.3 ℃ and release thermal energy when the temperature is lower than 37.2 ℃. It is clear in Fig. 4 that the TPCM also has a single and blunt peak in each melting and freezing curve. Similar to the phase change properties of the SPCM, the latent heat of the TPCM reaches up to 127.7-130.2 J/g with the phase temperature at 38.5-47.8 ℃ shown in Table 2. Different from pristine PEG, the SPCM and TPCM keep solid during the phase change process.

To further affirm the effect of crosslinking structure on enthalpy, the theoretical latent heats are calculated based on the weight percentage of PEG in solid-solid PCMs. The experimental value and theoretical value of latent heats for SPCM and TPCM are shown in Fig. 5. The theoretical values of melting and freezing latent heats are calculated by equation 1 and 2, respectively.

$$\Delta H_{tm} = \Delta H_{tPEG} \times \omega_{PEG} \quad (1)$$

$$\Delta H_{tf} = \Delta H_{fPEG} \times \omega_{PEG} \quad (2)$$

where ΔH_{tm} and ΔH_{tf} are the theoretical values of melting and freezing latent heats for solid-solid PCMs, J/g; ΔH_{tPEG} and ΔH_{fPEG} are the experimental values of melting and freezing latent heats for pristine PEG, J/g; ω_{PEG} is the weight percentage of PEG in solid-solid PCMs.

It is clear in Fig. 5 a and b that the experimental values of the melting and freezing

latent heats from SPCM and TPCM are equal to about 60 % of the theoretical counterparts, further confirming the defective crystallization and the small grain in Fig. 3. The poly(ethylene oxide) soft segments of solid-solid PCMs will be refined leading to the defective crystallization after the prepolymer derived from PEG and MDI-50 react with the trihydroxy Span 80 and Tween 80.

3.4 Thermal reliability of solid-solid PCMs

The DSC curves of the synthesized SPCM and TPCM after 100 thermal cycling are shown in Fig. 6. As can be seen from Fig. 6, the DSC curves of the solid-solid PCMs have small variation, and the phase change temperatures of SPCM and TPCM after thermal cycling are in accordance with that of SPCM and TPCM before thermal cycling. The melting latent heats before and after thermal cycling and loss ratio of latent heats of solid-solid PCMs are presented in Table 3 and the freezing latent heats before and after thermal cycling and loss ratio of latent heats before and after thermal cycling of solid-solid PCMs are shown in Table 4. Loss ratio of latent heats (*LR*) is calculated by equation 3. From Table 3 the melting *LR*s of SPCM and TPCM decrease by 8 % and 1.33 % respectively and Table 4 shows the freezing *LR*s reduce by 14.5 % and 0 % respectively. These results indicate the latent heats of the SPCM and TPCM after thermal cycling drop to some extent, having a negligible effect on a practical application. Base on these results, it can be concluded that the synthesized SPCM and TPCM have good thermal reliability.

$$LR = (\Delta H_b - \Delta H_a) / \Delta H_b \quad (3)$$

where *LR* is the loss ratio of latent heats of solid-solid PCMs, %; ΔH_b and ΔH_a are respectively the latent heats of solid-solid PCMs before and after thermal cycling, J/g.

FTIR spectra of SPCM and TPCM before and after thermal cycling are shown in Fig. 7. When the FTIR spectra of SPCM and TPCM compared in Fig. 7, it can be seen that the absorption peak positions and shapes do not vary after 100 thermal cycling, meaning that SPCM and TPCM have good chemical stability in terms of 100 thermal cycling.

3.5 Thermal stability of solid-solid PCMs

To study the thermal stability of solid-solid PCMs, the TG analysis was performed under the same conditions (i.e. heating rate of 10 ℃/min and nitrogen atmosphere) as most previous literatures.[1,3,20,27,35] For TES applications, the thermal stability of solid-solid PCMs is a very significant parameter due to the negative effect of thermal degradation on the working life of solid-solid PCMs. Fig. 8 shows the TG and DTG curves of PEG, SPCM and TPCM. As can be seen in Fig. 8 a and b, the pristine PEG exhibits one step thermal degradation that starts at 356 ℃ and ends completely at 403 ℃. However, the SPCM and TPCM involved the two-step mechanism of thermal degradation. When the temperature reaches 312 ℃, slight thermal degradation appears. It only decreases by 10 wt% once the temperature reaches 374 ℃. The SPCM and TPCM mainly degrade in the temperature range of 374-418 ℃. The maximum degradation rate appears at 387 ℃ for pristine PEG and at 396-399 ℃ for SPCM and TPCM shown in Fig. 8b. Compared with the pristine PEG, the main

degradation temperature of the SPCM and TPCM increases by 18 ℃, meaning the thermal stability of the SPCM and TPCM is higher than that of the PEG. Concluded from the above results, the synthesized SPCM and TPCM do not degrade below 312 ℃ and the prepared solid-solid PCMs (i.e. SPCM and TPCM) have good thermal stability.

4. Conclusions

The SPCM and TPCM have been synthesized as new solid-solid PCMs by bulk polycondensation in the absence of organic solvents. The PEG works as phase change material in the solid-solid SPCM and TPCM. The Span 80 and Tween 80 are used as crosslinking agents in the polyurethane synthesis for the first time. The reaction of PEG, Span 80 and Tween 80 with MDI-50 was confirmed by FTIR. The XRD investigations show the SPCM and TPCM have a completely crystalline structure. Because of crosslinking structure, the SPCM and TPCM reflect the defective crystallization and the small grains leading to the lower experimental latent heats than theoretical latent heats by calculation. The DSC results exhibit that the fabricated SPCM and TPCM have proper phase change temperatures of 37-48 ℃ and high latent heats in the range of 120 -130 J/g. It can be confirmed from the accelerated thermal cycling testing that the SPCM and TPCM possess good thermal reliability and chemical stability. From TG results, the SPCM and TPCM do not degrade below 312 ℃, meaning that the synthesized SPCM and TPCM have good thermal stability.

References

1 F. He, X. Wang and D. Wu, Phase-change characteristics and thermal performance of form-stable n-alkanes/silica composite phase change materials fabricated by sodium silicate precursor, *Renew. Energ.*, 2015, **74**, 689-698.

2 X. Fang, L. Fan, Q. Ding, X. Yao, Y. Wu, J. Hou, X. Wang, J. Yu, G. Cheng and Y. Hu, Thermal energy storage performance of paraffin-based composite phase change materials filled with hexagonal boron nitride nanosheets, *Energ. Convers. Manage.,* 2014, **80**, 103-109.

3 Y. Konuklu, Microencapsulation of phase change material with poly(ethylacrylate) shell for thermal energy storage, *Int. J. Energ. Res.,* 2014, **38**, 2019-2029.

4 D. Simon, J. Rodriguez, P. Sanchez and L. Sanchez-Silva, The effect of the dry glass transition temperature on the synthesis of paraffin microcapsules obtained by suspension-like polymerization, *Polym. Eng. Sci.,* 2014, **54**, 208-214.

5 X. Yang, Y. Yuan, N. Zhang, X. Cao and C. Liu, Preparation and properties of myristic–palmitic–stearic acid/expanded graphite composites as phase change materials for energy storage, *Sol. Energy,* 2014, **99**, 259-266.

6 B. Xu and Z. Li, Performance of novel thermal energy storage engineered cementitious composites incorporating a paraffin/diatomite composite phase change material, *Appl. Energ.,* 2014, **121**, 114-122.

7 Z. Zhang, X. Fang, Study on paraffin/expanded graphite composite phase change thermal energy storage material, *Energ. Convers. Manage.*, 2006, **47**, 303-310.

8 P. Goli, S. Legedza, A. Dhar, R. Salgado, J. Renteria and A. Balandin,

Graphene-enhanced hybrid phase change materials for thermal management of Li-ion batteries, *J. Power. Sources.,* 2014, **248**, 37-43.

9 Y. Zhang, S. Wang, Z. Rao and J. Xie, Experiment on heat storage characteristic of microencapsulated phase change material slurry, *Sol. Energ. Mat. Sol. C*., 2011, **95**, 2726-2733.

10 T. Kousksou, A. Jamil, T. E. Rhafiki and Y. Zeraouli, Paraffin wax mixtures as phase change materials, *Sol. Energ. Mat. Sol. C*., 2010, **9**4, 2158-2165.

11 X. Li, J. Sanjayan and J. Wilson, Fabrication and stability of form-stable diatomite/paraffin phase change material composites, *Energ. Buildings*, 2014, **76**, 284-294.

12 M. M. Farid, A. M. Khudhair, S. A. K. Razack and S. Al-Hallaj, A review on phase change energy storage: materials and applications, *Energ. Convers. Manage.,* 2004, **45**, 1597–1615.

13 Z. Chen, F. Yu, X. Zeng and Z. Zhang, Preparation, characterization and thermal properties of nanocapsules containing phase change material n-dodecanol by miniemulsion polymerization with polymerizable emulsifier, *Appl. Energy*, 2012, **91**, 7-12.

14 J. Giro-Paloma, G. Oncins, C. Barreneche, M. Martínez, A. Inés Fernández and L. F. Cabeza, Physico-chemical and mechanical properties of microencapsulated phase change material, *Appl. Energ.*, 2013, **109**, 441-448.

15 J. Li, P. Xue, W. Ding, J. Han and G. Sun, Micro-encapsulated paraffin/high-density polyethylene/wood flour composite as form-stable phase change

material for thermal energy storage, *Sol. Energ. Mat. Sol. C.*, 2009, **93**, 1761-1767.

16 C. Alkan and A. Sari, Fatty acid/poly(methyl methacrylate) (PMMA) blends as form-stable phase change materials for latent heat thermal energy storage, *Sol. Energy*, 2008, **82**, 118-124.

17 Y. Özonur, M. Mazman, H. Ö. Paksoy and H. Evliya, Microencapsulation of coco fatty acid mixture for thermal energy storage with phase change material, *Int. J. Energ. Res.*, 2006, **30**, 741-749.

18 C. Alkan, E. Gunther, S. Hiebler, O. Ensari and D. Kahraman, Polyurethanes as solid–solid phase change materials for thermal energy storage, *Sol. Energy,* 2012, **86**, 1761-1769.

19 K. Chen, R. Liu, C. Zou, Q. Shao, Y. Lan and X. Cai, Linear polyurethane ionomers as solid–solid phase change materials for thermal energy storage, *Sol. Energ. Mat. Sol. C.*, 2014, **130**, 466-473.

20 C. Chen, W. Liu, Z. Wang, K. Peng, W. Pan and Q. Xie, Novel form stable phase change materials based on the composites of polyethylene glycol/polymeric solid-solid phase change material, *Sol. Energ. Mat. Sol. C.*, 2015, **134**, 80-88.

21 X. Qiu, W. Li, G. Song, X. Chu and G. Tang, Microencapsulated n-octadecane with different methylmethacrylate-based copolymer shells as phase change materials for thermal energy storage, *Energy*, 2012, **46**, 188-199.

22 Y. Wang, T. Xia, H. Feng and Zhang H, Stearic acid/polymethylmethacrylate composite as form-stable phase change materials for latent heat thermal energy storage, *Renew. Energ.,* 2011, **36**, 1814-1820.

23 M. Jonsson, O. Nordin, E. Malmstrom and C. Hammer, Suspension polymerization of thermally expandable core/shell particles, *Polymer*, 2006, **47**, 3315-3324.

24 A. Sarı, C. Alkan, A. Bicer and A. Karaipekli, Synthesis and thermal energy storage characteristics of polystyrene-graft-palmitic acid copolymers as solid-solid phase change materials, *Sol. Energ. Mat. Sol. C.*, 2011, **95**, 3195–3201.

25 J. Su and P. Liu, A novel solid–solid phase change heat storage material with polyurethane block copolymer structure, *Energ. Convers. Manage.,* 2006, **47**, 3185–3191.

26 A. Sarı, C. Alkan and A. Bicer, Synthesis and thermal properties of polystyrene-graft-PEG copolymers as new kinds of solid–solid phase change materials for thermal energy storage, *Mater. Chem. Phys.*, 2012, **133**, 87–94.

27 C. Chen, W. Liu, H. Wang and K. Peng, Synthesis and performances of novel solid–solid phase change materials with hexahydroxy compounds for thermal energy storage, *Appl. Energ.*, 2015, **152**, 198-206.

28 P. Xi, L. Xia, P. Fei, D. Zhang and B. Cheng, Preparation and performance of a novel thermoplastics polyurethane solid–solid phase change materials for energy storage, *Sol. Energ. Mat. Sol. C.*, 2012, **102**, 36–43.

29 D. Zhou, C. Zhao and Y. Tian, Review on thermal energy storage with phase change materials (PCMs) in building applications, *Appl. Energ.*, 2012, **92**, 593-605.

30 C Chen, Y Zhao and W Liu, Electrospun polyethylene glycol/cellulose acetate phase change fibers with core–sheath structure for thermal energy storage, *Renew. Energy.*, 2013, **60**, 222-225.

31 C. A. Whitman, M. B. Johnson and M. A. White, Characterization of thermal performance of a solid–solid phase change material, di-n-hexylammonium bromide, for potential integration in building materials, *Thermochim. Acta.*, 2012, **531**, 54-59.

32 Q. Cao and P. Liu, Crystalline-amorphous phase transition of hyperbranched polyurethane phase change materials for energy storage, *J. Mater. Sci.*, 2007, **42**, 5661-5665.

33 X. Zhou, Preparation and characterization of PEG/MDI/PVA copolymer as solid–solid phase change heat storage material, *J. Appl. Polym. Sci.*, 2009, **113**, 2041–2045.

34 C. Chen, W. Liu, H. Yang, Y. Zhao and S. Liu, Synthesis of solid–solid phase change material for thermal energy storage by crosslinking of polyethylene glycol with poly(glycidyl methacrylate), *Sol. Energy*, 2011, **85**, 2679-2685.

35 K. Chen, X. Yu, C. Tian and J. Wang, Preparation and characterization of form-stable paraffin/polyurethane composites as phase change materials for thermal energy storage, *Energ. Convers. Manage.*, 2014, **77**, 13-21.

Figure captions

Table 1 The detailed compositions of PEG, Span 80 and Tween 80 from FTIR.

Table 2 Phase change results of PEG and solid-solid PCMs from DSC curves.

Table 3 Melting latent heat before and after thermal cycling and loss ratio of latent heat of solid-solid PCMs.

Table 4 Freezing latent heat before and after thermal cycling and loss ratio of latent

heat of solid-solid PCMs.

Fig. 1 Synthetic route of solid-solid PCMs.

Fig. 2 FTIR spectra of (a) PEG, (b) Span 80, (c) Tween 80, (d) SPCM and (e) TPCM.

Fig. 3 XRD curves of PEG, SPCM and TPCM.

Fig. 4 DSC curves of PEG, SPCM and TPCM.

Fig. 5 Experimental values and theoretical values of melting (a) and freezing (b) latent heats for solid-solid PCMs.

Fig. 6 DSC curves of solid-solid PCMs before and after thermal cycling.

Fig. 7 FTIR spectra of solid-solid PCMs before (solid line) and after (dash dot dot line) 100 thermal cycling.

Fig. 8 TG (a) and DTG (b) curves of PEG, SPCM and TPCM.

Table 1 The detailed compositions of PEG, Span 80 and Tween 80 from FTIR.

Characteristic vibration	Characteristic peaks (cm^{-1})
PEG	
O-H stretching	3481
C-H stretching	2888
C-H bending	1467, 1342, 1280, 1242
C-O stretching	1101
C-H deformation	962, 842
Span 80	
O-H stretching	3399
C-H stretching	2925, 2855
C=O stretching	1739
C-H bending	1459, 1374
C-O stretching	1173, 1085
Tween 80	
O-H stretching	3428
C-H stretching	2923, 2863
C=O stretching	1735
C-H bending	1460, 1352, 1249
C-O stretching	1107
C-H deformation	948, 842

Table 2 Phase change results of PEG and solid-solid PCMs from DSC curves.

Sample	ΔH_m (J/g)	T_m (℃)	ΔH_c (J/g)	T_c (℃)
PEG	234.4	59.7	248.1	39.6
SPCM	122.4	44.3	120.3	37.2
TPCM	127.7	47.8	130.2	38.5

Table 3 Melting latent heat before and after thermal cycling and loss ratio of latent heat of solid-solid PCMs.

Solid-solid PCMs	Melting latent heat before thermal cycling (J/g)	Melting latent heat after thermal cycling (J/g)	Loss ratio of latent heat (%)
SPCM	122.4	112.6	8.00
TPCM	127.7	126.0	1.33

Table 4 Freezing latent heat before and after thermal cycling and loss ratio of latent heat of solid-solid PCMs.

Solid-solid PCMs	Freezing latent heat before thermal cycling (J/g)	Freezing latent heat after thermal cycling (J/g)	Loss ratio of latent heat (%)
SPCM	120.3	102.8	14.5
TPCM	130.2	130.2	0

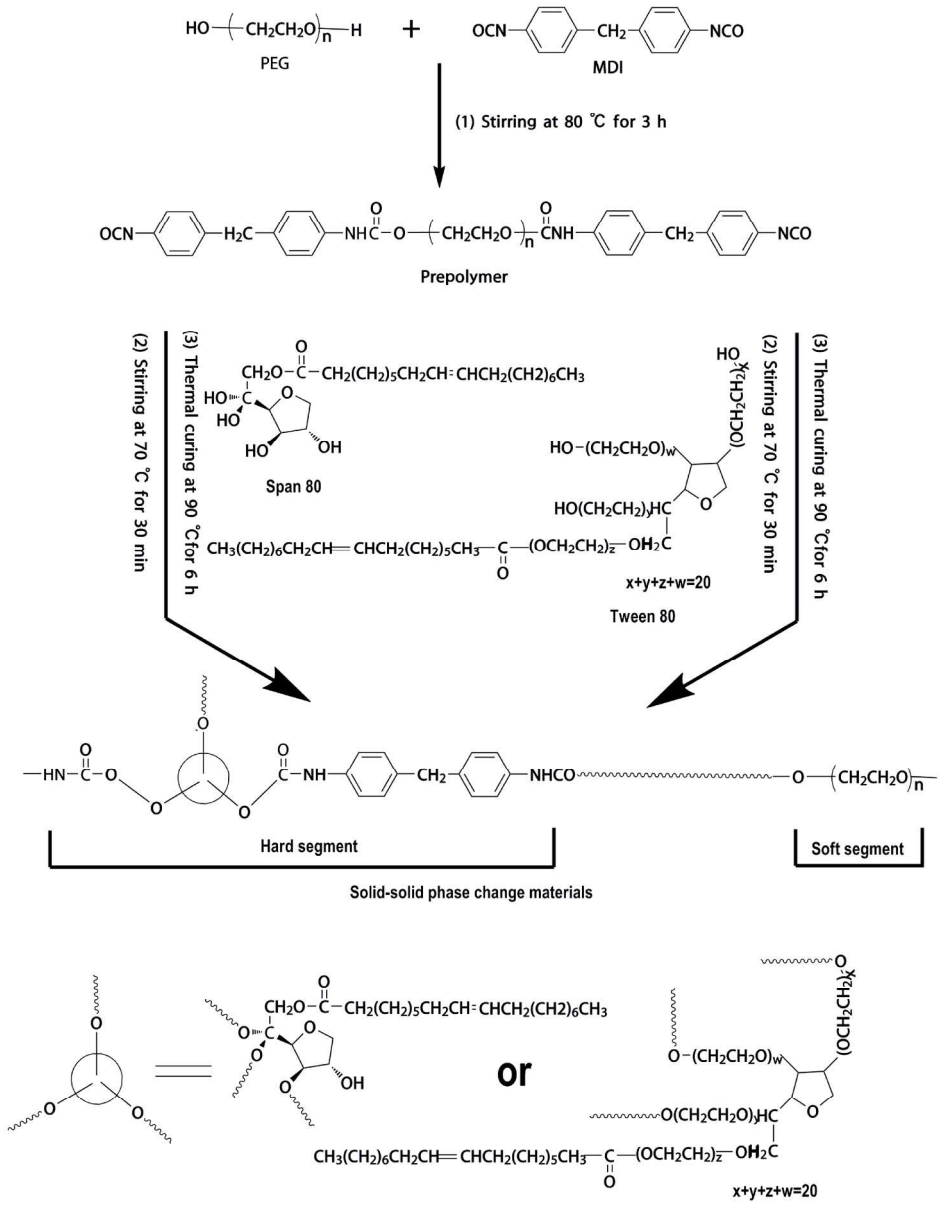

Fig. 1 Synthetic route of solid-solid PCMs.
191x245mm (300 x 300 DPI)

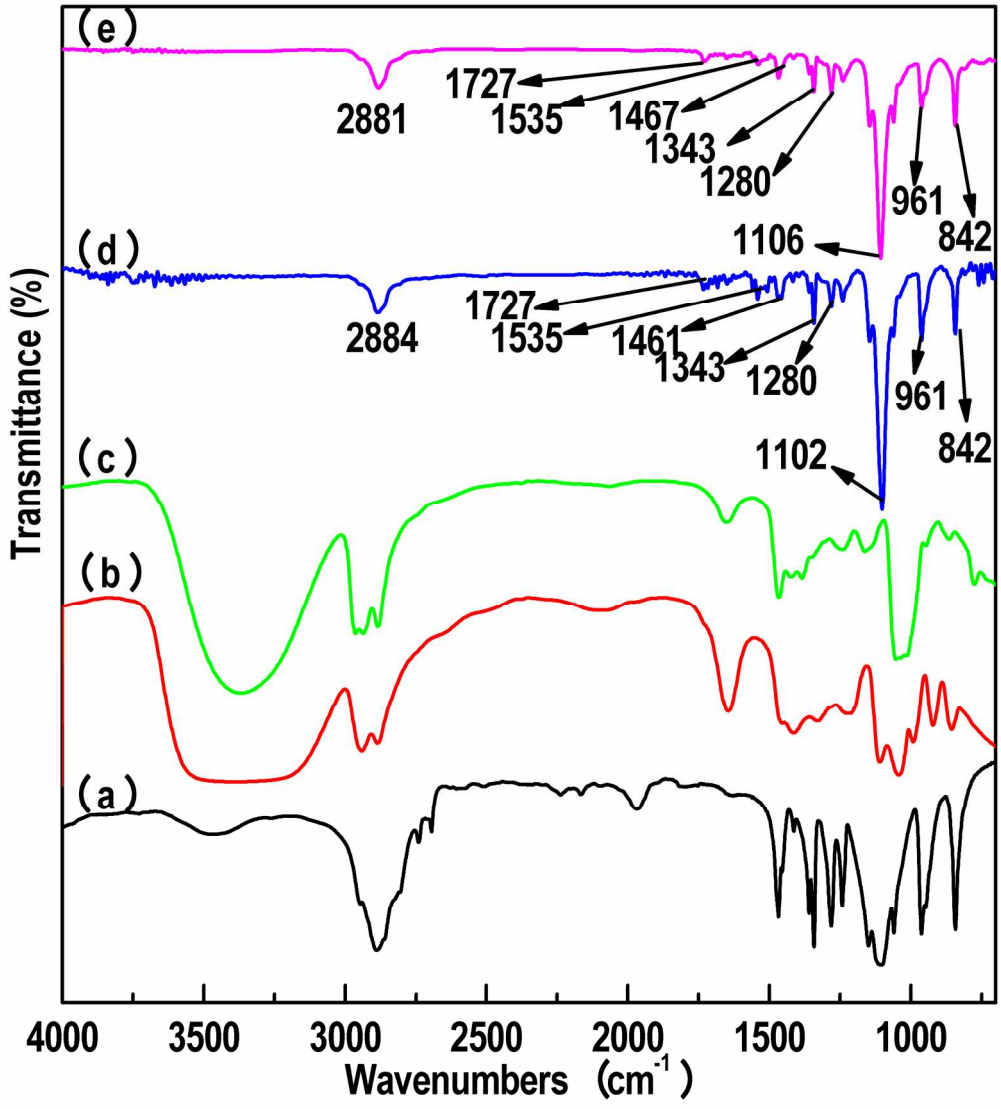

Fig. 2 FTIR spectra of (a) PEG, (b) Span 80, (c) Tween 80, (d) SPCM and (e) TPCM.
93x103mm (600 x 600 DPI)

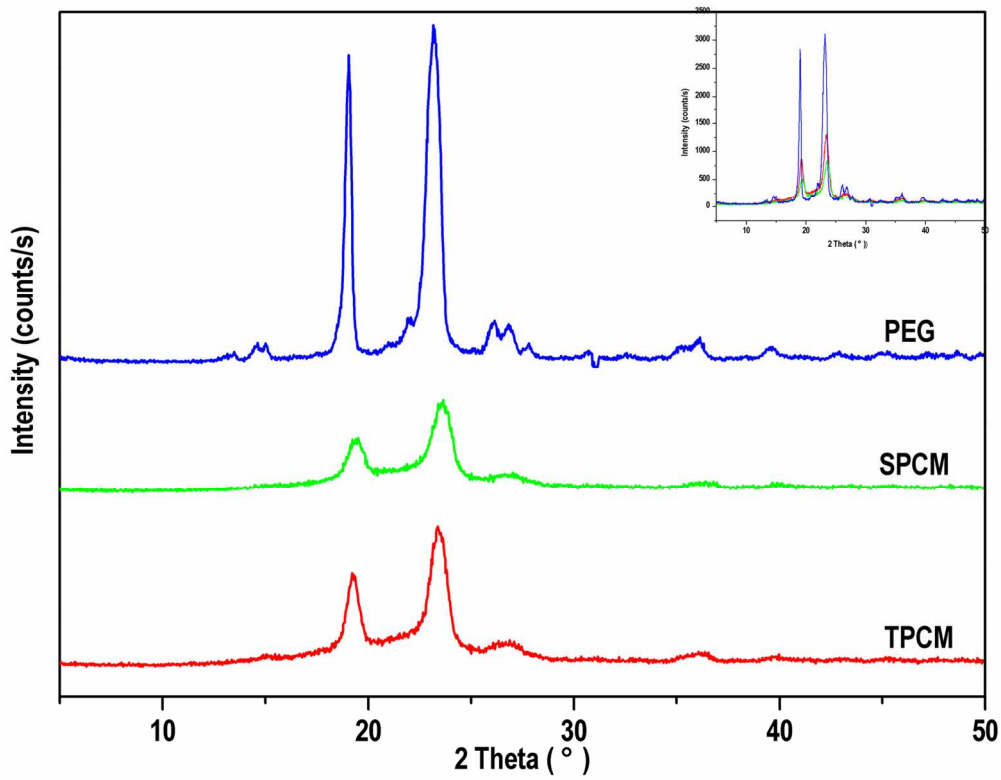

Fig. 3 XRD curves of PEG, SPCM and TPCM.
65x51mm (600 x 600 DPI)

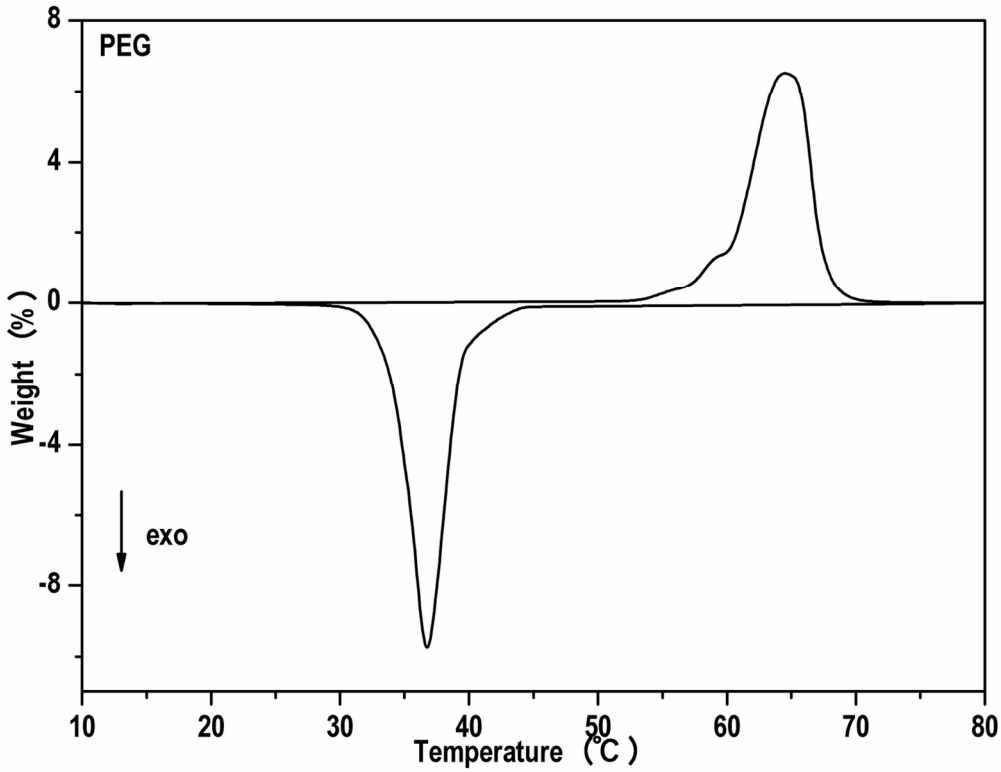

Fig. 4a DSC curves of PEG.
65x50mm (600 x 600 DPI)

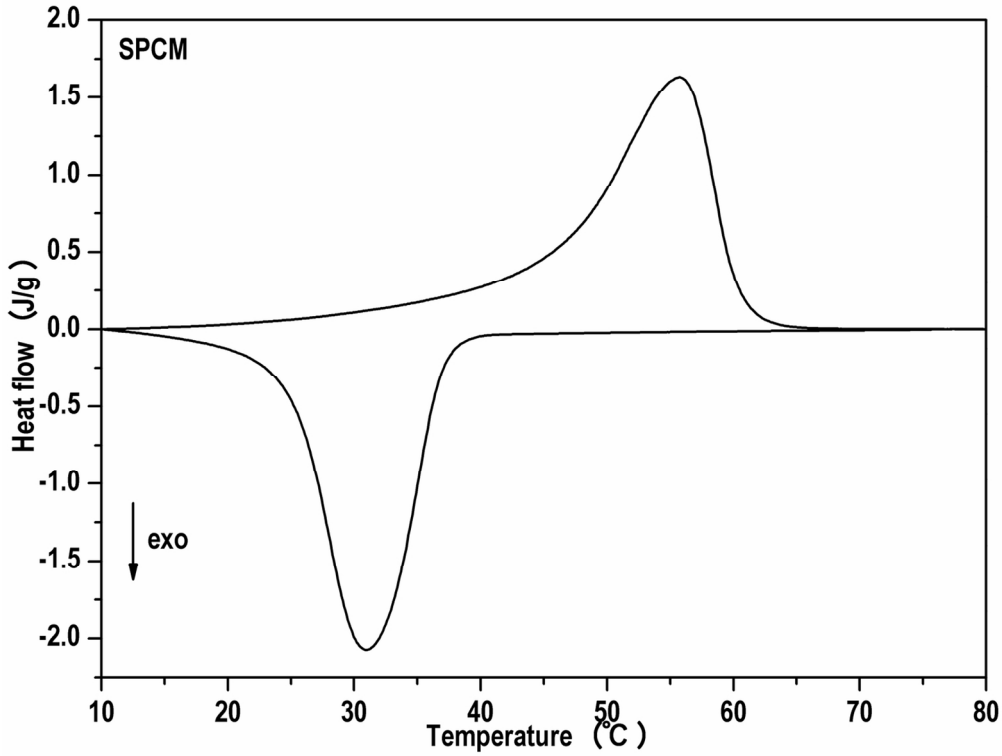

Fig. 4b DSC curves of SPCM.
64x48mm (600 x 600 DPI)

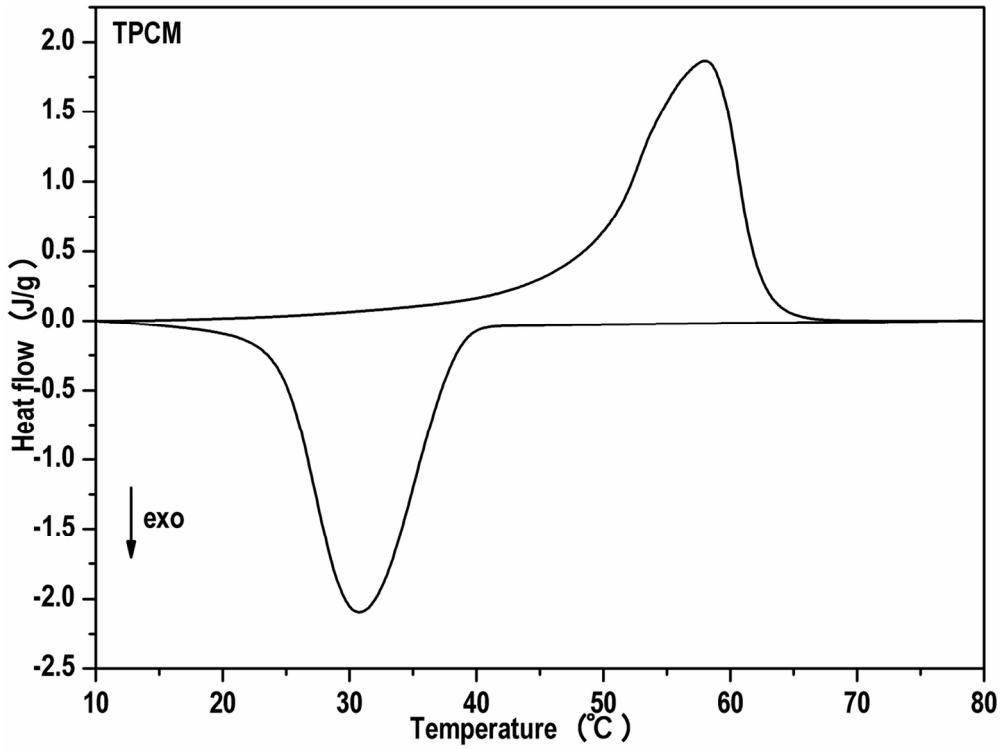

Fig. 4c DSC curves of TPCM.
63x46mm (600 x 600 DPI)

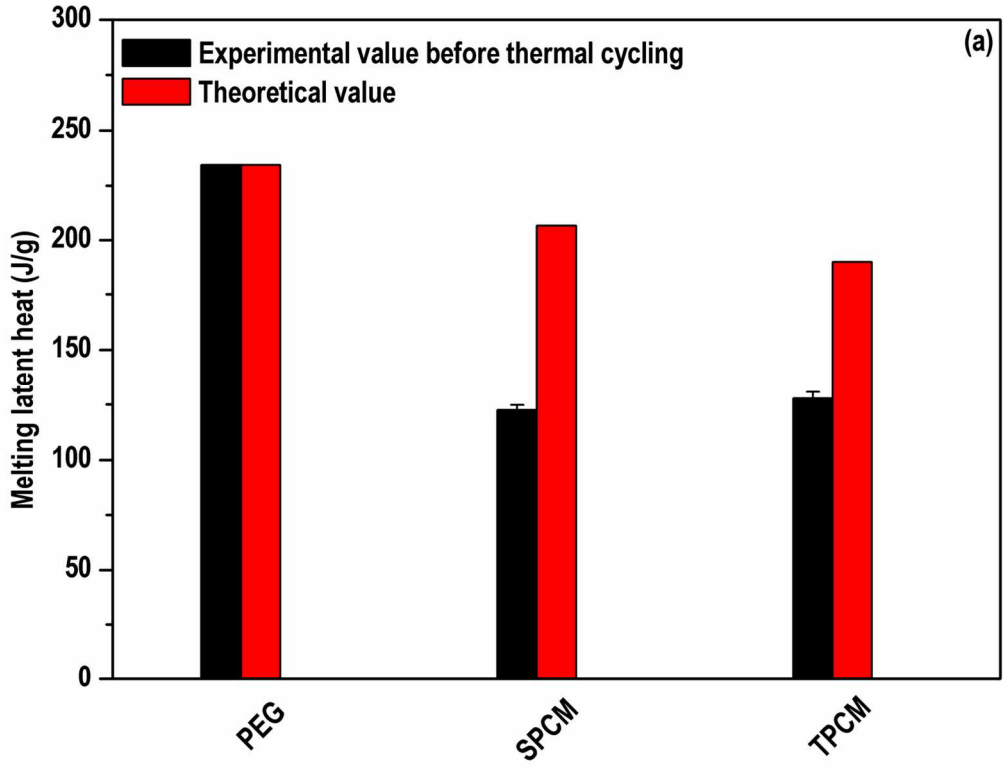

Fig. 5a Experimental values and theoretical values of melting latent heat for solid-solid PCMs.
65x51mm (600 x 600 DPI)

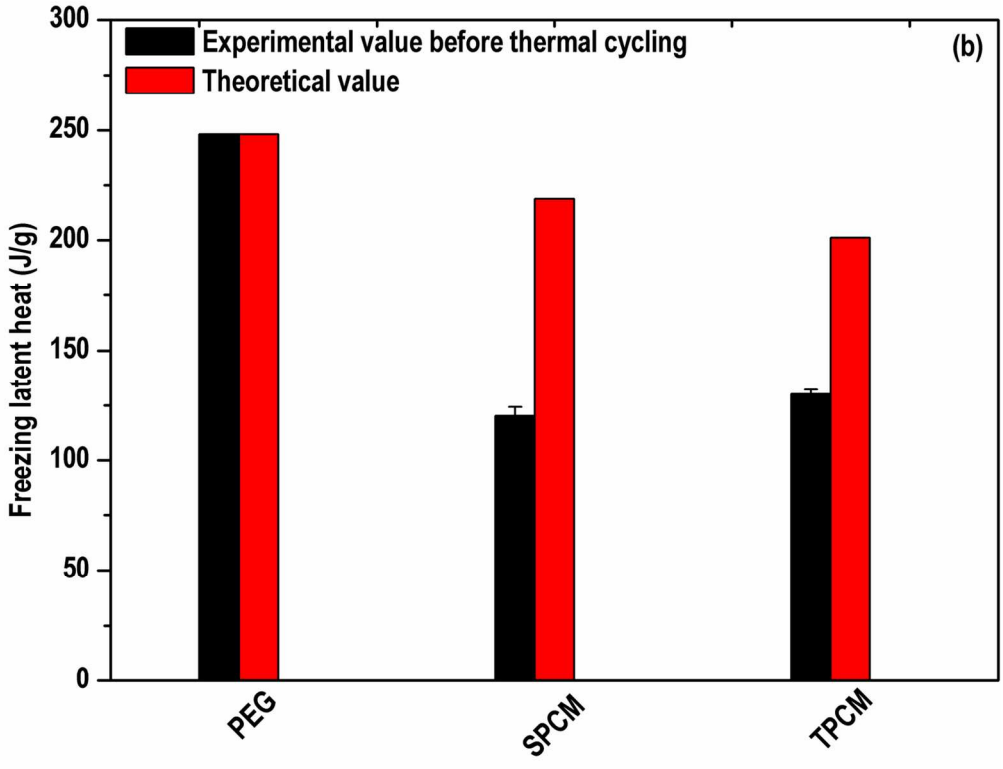

Fig. 5b Experimental values and theoretical values of freezing (b) latent heats for solid-solid PCMs.
65x50mm (600 x 600 DPI)

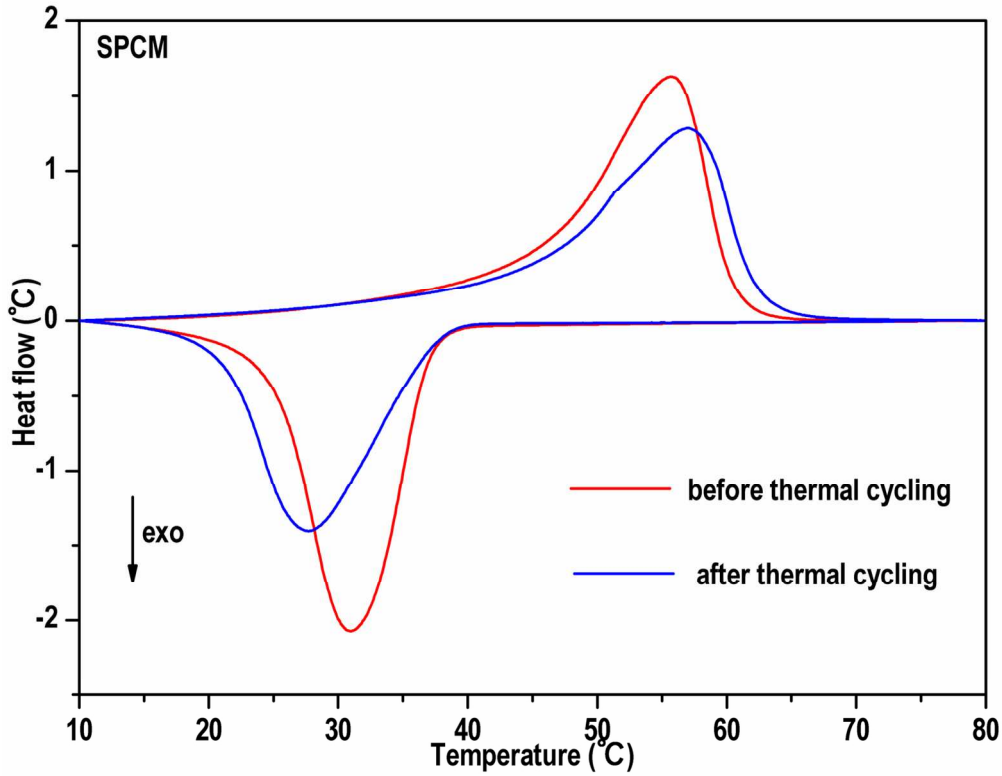

Fig. 6a DSC curves of SPCM before and after thermal cycling.
66x51mm (600 x 600 DPI)

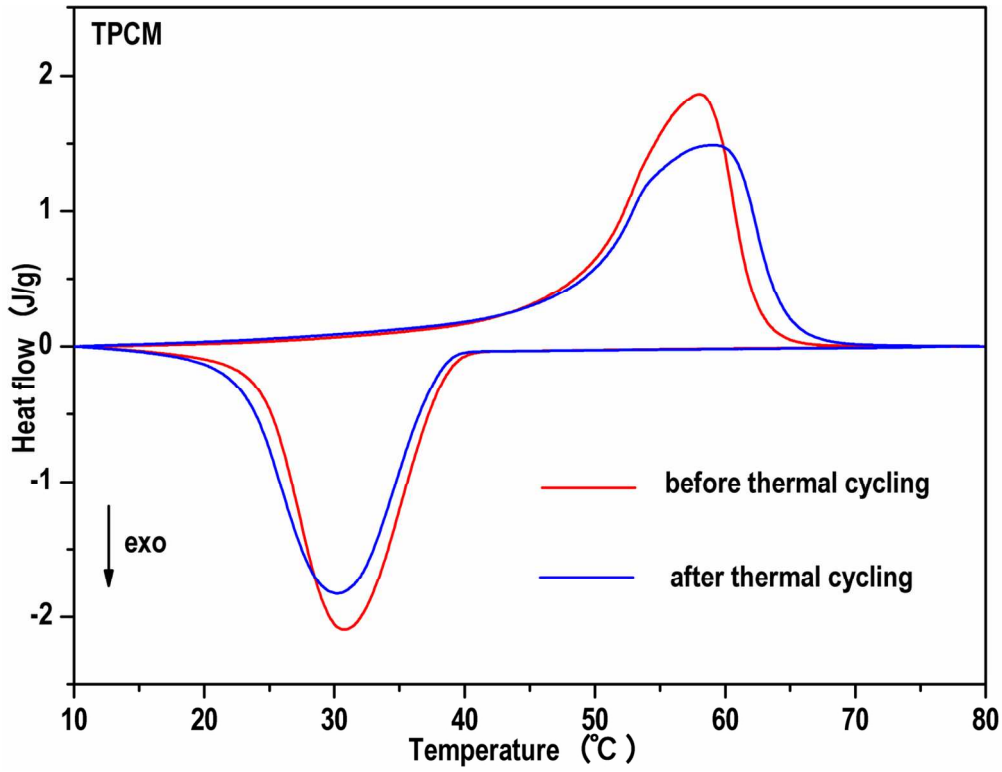

Fig. 6b DSC curves of TPCM before and after thermal cycling.
64x49mm (600 x 600 DPI)

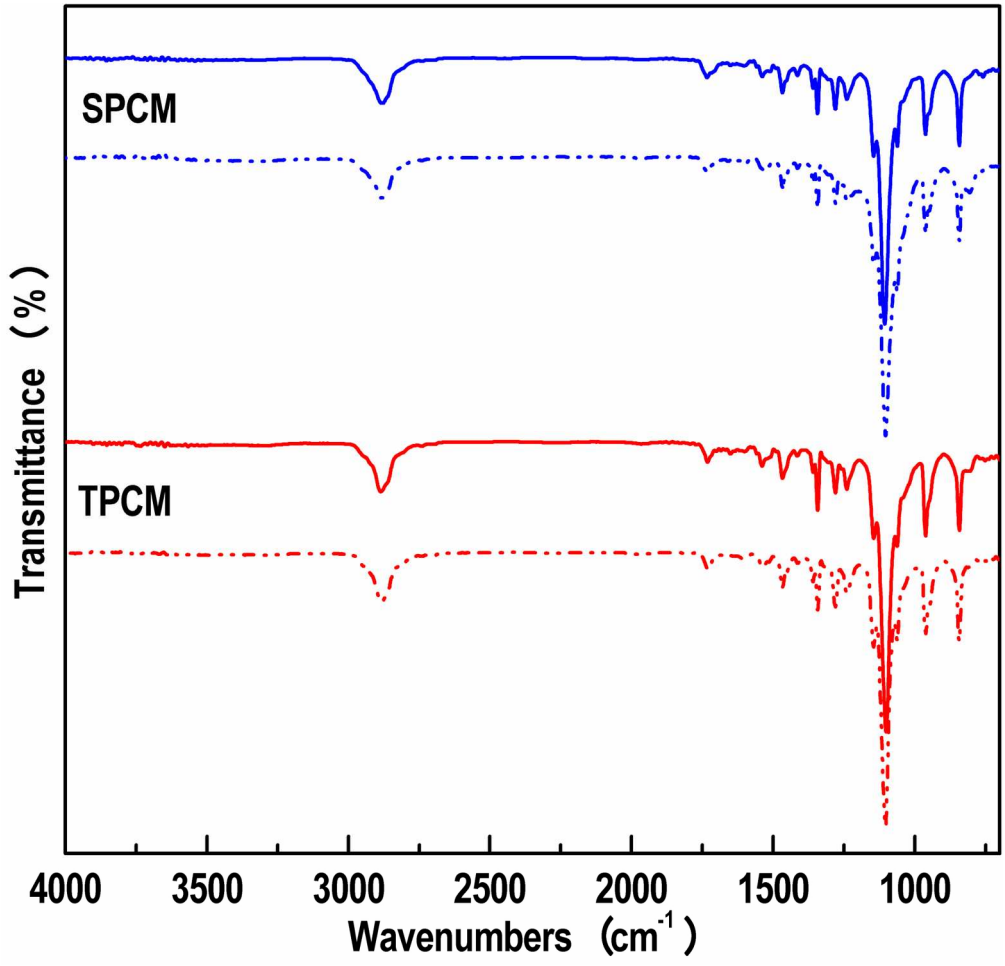

Fig. 7 FTIR spectra of solid-solid PCMS before (solid line) and after (dash dot dot line) 100 thermal cycling.
81x78mm (600 x 600 DPI)

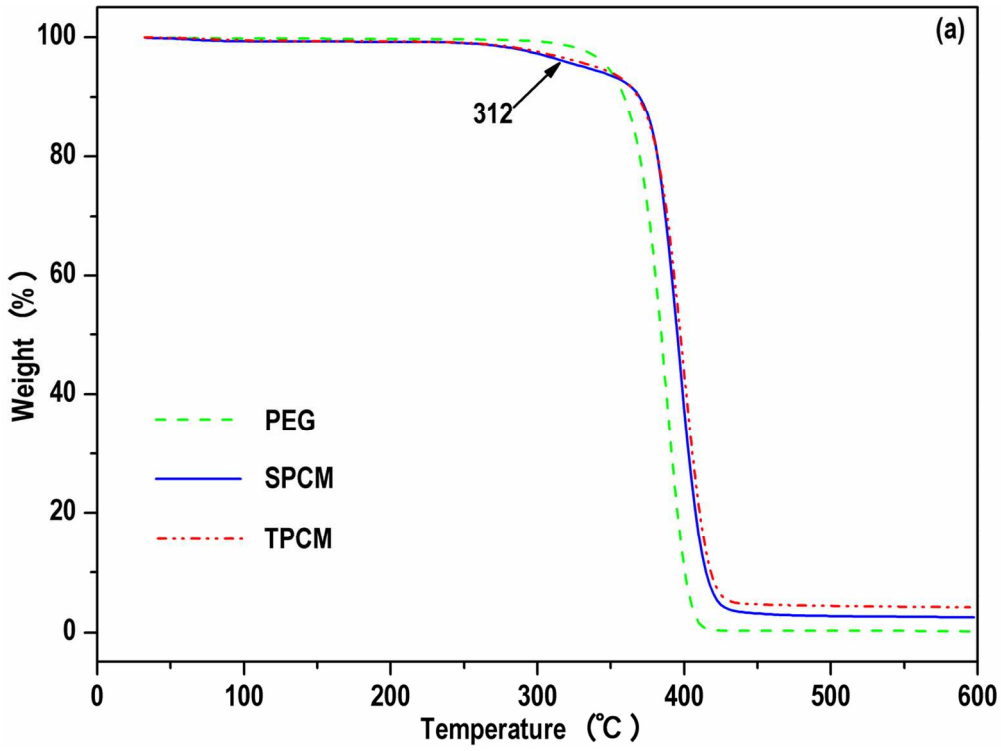

Fig. 8a TG curves of PEG, SPCM and TPCM.
63x46mm (600 x 600 DPI)

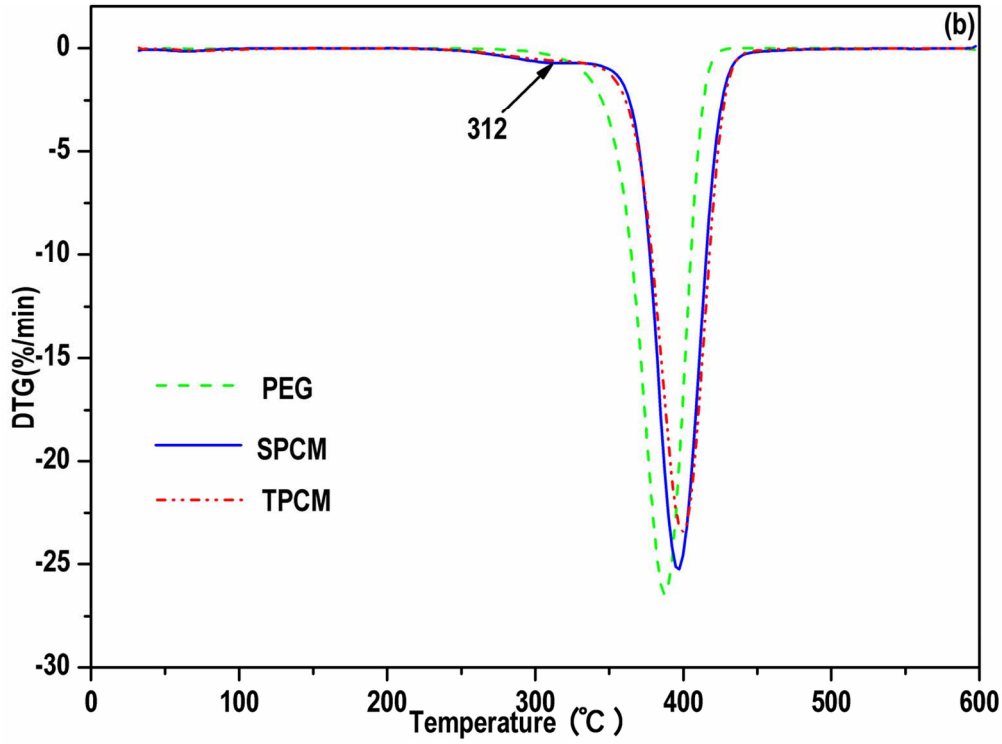

Fig. 8b DTG curves of PEG, SPCM and TPCM.
62x46mm (600 x 600 DPI)